Article

Not peer-reviewed version

Vortex Characterisation and Parametric Study of Miniature Vortex Generators and Their Near Field Boundary Layer Effects

Gilles De Baets , András Szabó , Péter Tamás Nagy , György Paál , Maarten Vanierschot *

Posted Date: 26 July 2024

doi: 10.20944/preprints202407.2164.v1

Keywords: Drag reduction; Boundary layer interaction; Miniature Vortex Generator; Transition delay

Article

Vortex Characterisation and Parametric Study of Miniature Vortex Generators and Their Near Field Boundary Layer Effects

Gilles De Baets [1], Andras Szabó [2], Péter Tamás Nagy [2], György Paál [2] and Maarten Vanierschot [1,3,*]

1 KU Leuven, Department of Mechanical Engineering, B-3001 Leuven, Belgium; gilles.debaets@kuleuven.be
2 Budapest University of Technology and Economics, Department of Hydrodynamic Systems, Budapest, H-1111, Hungary;
3 North-West University, Material Science, Innovation and Modelling (MaSIM), Mmabatho 2745, South Africa
* Correspondence: maarten.vanierschot@kuleuven.be

Abstract: Delaying the onset of laminar-turbulent transition is an attractive method in reducing skin friction drag, especially on streamlined bodies where Tollmien-Schlichting instabilities are the dominating mechanism for transition. Miniature vortex generators (MVGs) offer an effective approach to attenuate these instabilities by generating counter-rotating vortex pairs. They are placed in pairs within an array and resemble small winglet-type elements. The conventional methodology involves adjusting MVG parameters and conducting computationally expensive DNS and/or downstream stability analyses to assess their effectiveness. However, analyzing the vortex parameters of MVG-generated vortices can potentially guide a more targeted approach in modifying MVG parameters and identifying critical factors for transition delay. Therefore, this study investigates changes in three primary MVG parameters, namely inner distance, periodicity and height, and utilizes computational fluid dynamics (CFD) analysis to create a dataset that examines the characteristics of the generated counter-rotating vortex pairs and their potential in drag reduction. The objective is to establish correlations among these parameters and their influence on delaying transition.

Keywords: drag reduction; boundary layer interaction; miniature vortex generator; transition delay

---

1. Introduction

Efficient energy usage is a key aspect in our efforts to reduce greenhouse gas emissions and increase powertrain efficiencies around the world. A substantial part of global energy consumption is dedicated to transportation. Here, aerodynamic drag plays a critical role, significantly impacting the energy consumption in this sector, which is still largely dominated by fossil fuels. Reducing drag forces involves overcoming two main types of drag: pressure drag and skin friction drag. For streamlined objects, skin friction forces typically outweigh pressure forces, making the reduction of skin friction drag the most appealing. However, skin friction, inherently tied to the boundary layer flow of a fluid over a surface, is particularly challenging to reduce. A closer examination reveals that laminar boundary layers have significantly lower skin friction than turbulent boundary layers. As the Reynolds number (Re) increases, there is a rapid rise in the skin friction coefficient (C_f), further complicating the effort to minimize drag. Delaying the transition from laminar to turbulent flow results in a net lower skin friction drag, but the mechanisms governing this transition are complex and depend on the type of flow and environmental factors.

These transition mechanisms, first described by Reynolds at the end of the 19th century, are since well studied. In case of boundary layer flow, two main classes of transition are described: one describing a natural transition while the other one describing a bypass approach [1], [2]. When there is no modal growth observed during transition, it can be categorised as "bypass" transition. This type is most often due to the growth of an initial perturbation, e.g. free stream disturbances or surface

 doi:10.20944/preprints202407.2164.v1

roughness. Its nonmodal method bypasses the modal growth as seen in the former category, the natural transition. This transition is found when there are no or only very small environmental disturbances. This modal approach is distinguished by exponential amplification (or decay) of disturbances within a certain range of forcing frequencies and Re numbers. The initial unstable eigenmode is characterized by exponentially growing travelling waves referred to as Tollmien-Schlichting (TS) waves [3] [4]. This research primarily concentrates on natural transition, as this boundary layer instability transition type is understood much better and is much more suitable for flow control. It is also more fundamentally and practically significant for addressing challenges related to real-life applications such as moving vehicles in cruise conditions. A significant body of research is devoted to active methods of attenuating these T-S waves, such as suction systems, wall motion or surface heating [5]. However, a passive method proves to be more attractive, as this mitigates the need for additional energy-consuming parts such as sensors or actuators, making it much easier to practically implement. In this field, pioneering work by Fransson *et al.* [6] showed that creating streamwise elongated streaks can effectively dampen the growth of these TS waves in such a way that postponing transition is possible. This streak generation however is an intricate mechanism that, if not carefully controlled, could create the opposite effect, i.e. advancing the transition location. The fundamental process behind transition delay is the "lift-up" mechanism, as described in [7]. Streaks are created by a relatively weak pair of streamwise vortices that are counter-rotating. The resulting low and high speed spanwise velocity variations are created by the alternating effect of lifting up the low speed fluid from the near-wall boundary region, and the down pulling of the higher speed velocity region of the upper boundary layer. This interchange of momentum leads to the formation of streaks. These varying slow-fast regions create spanwise shear in the boundary layer, which is the main mechanism in decreasing the disturbance energy growth, essentially dampening the TS waves and postponing the transition location [8][9]. Both experimental work [10] and numerical simulations [8] has shown that appropriate streak generation has the capability of attenuating TS wave growth, with the main factor that influences the effectiveness of this attenuation being the streak amplitude [11]. A high amplitude is sought after for its stabilizing effect, however there is a balance to maintain: when this amplitude crosses a critical threshold, the streaks can cause secondary instabilities, effectively advancing the transition location. Different methods exist for creating this streaky boundary layer pattern. Initially, circular and rectangular roughness elements have been investigated, both proving effective [10,12–14]. However, currently the most promising method of streak generation are a small winglet-type elements that create these counter rotating vortices. These are called Miniature Vortex Generators or MVGs. They differ from "classical" vortex generators, which are used to delay separation, as they are smaller and present in the laminar region of the boundary layer. The main body of work showing the effectiveness of these MVGs are the experiments of Fransson and Shahinfar [15,16].

Previous works have done limited parametric studies investigating the influence of certain MVG parameters on the effects of streak generation downstream. Although idealized vortices, such as those proposed by Siconolfi *et al.* [17], offer the most control and adjustability over the initial flow field that induces the streaky boundary layer, they do not represent a realistic configuration. On the other hand, analyzing the effect of the MVG geometry on the streak amplitude provides valuable insight into the effectiveness of an MVG setup, yet it fails to demonstrate how the distinct characteristics of the vortex itself play a role. A knowledge gap persists: until now, physical MVG parameters have been altered to analyze streak generation, but no investigation has focused on the vortices themselves. While the numerical studies of Siconolfi *et al.* [17] examined the introduction of an idealized Batchelor vortex and its effect on downstream drag reduction, no vortex analysis has been performed on the vortices generated by the MVG pairs themselves. This study aims to bridge that gap. By analyzing vortex parameters, it is possible to gain insight into which characteristics influence drag reduction, and how these parameters of realistic vortices compare to well-defined idealized ones [18]. While some studies described relationships between MVG parameters and streak amplitude, the limited

Preprints.org (www.preprints.org) | NOT PEER-REVIEWED | Posted: 26 July 2024 doi:10.20944/preprints202407.2164.v1

range of configurations restricts the applicability of these findings. Building on the collaborative study conducted with Szabó *et al.* [19], further analyses are undertaken to extend the findings obtained in that research. This study will therefore perform a large parameter study, focusing on two key aspects: expanding the current parametric investigation of MVGs and characterizing the vortices generated by different MVG setups and their effect on drag reduction.

2. Materials and Methods

2.1. Governing equations and numerical setup

The analysis of the vortices generated by MVGs was done by first solving the steady-state 3D Navier-Stokes equations, which are based on the conservation of mass and momentum. These equations are represented as:

$$\begin{aligned} \nabla \cdot \mathbf{u} &= 0\,, \\ (\mathbf{u} \cdot \nabla)\mathbf{u} &= -\frac{1}{\rho}\nabla p + \nu \nabla^2 \mathbf{u}, \end{aligned} \tag{1}$$

where $\mathbf{u}$ denotes the velocity vector, t is time, p represents pressure, ρ is density, and ν stands for kinematic viscosity. Ansys Fluent 2020 R1 was used to solve these equations. The computational meshes used for the various configurations are consistent with those reported by Siconolfi *et al.* [9], maintaining a uniform height of 13 mm in all cases. Research by Camarri *et al.* [20] indicated that, provided the computational domain is adequately large, altering its size does not significantly impact the results. Figure 1 shows a schematic of the computational domain. The domain starts at X_0, with X_{MVG} indicating the center of the MVGs relative to the domain's beginning. To optimize computational efficiency, simulations were conducted for only half of the domain, corresponding to a single MVG from each MVG pair. A symmetry condition, as described by Camarri *et al.* [20], was applied in both sides of the domain for these simulations. A fully developed Blasius profile is implemented at the inlet in the wall-normal coordinate (y), while ensuring uniformity in the spanwise direction (z). The boundary layer thickness at the MVG location is $\delta_{99,MVG} = 3.610\,\text{mm}$. At the outlet, a pressure boundary condition is set with a gauge pressure of 0 Pa, which was also applied at the top boundary, with no velocity gradient perpendicular to the boundary. An overview of this is given in Figure 1. To maintain consistency across different cases, careful attention was given to avoid significant variations in mesh size or quality. The mesh is finest near the MVG and becomes progressively coarser further away. Typically, the mesh consists of approximately 3 to 5 million elements. It was verified that changes in mesh resolution have a negligible effect on the results, with a discretization error around 0.5%. The QUICK (Quadratic Upstream Interpolation for Convective Kinematics) scheme is used for discretizing momentum, while the PRESTO! scheme is employed for pressure discretization. The pressure-velocity coupling uses the segregated SIMPLEC (Semi-Implicit Method for Pressure Linked Equations-Consistent) method. Each simulation continues until the residuals achieve double-precision machine accuracy before concluding. For analysing the downstream drag reduction abilities, a BiGlobal stability analysis is performed, detailed in [19].

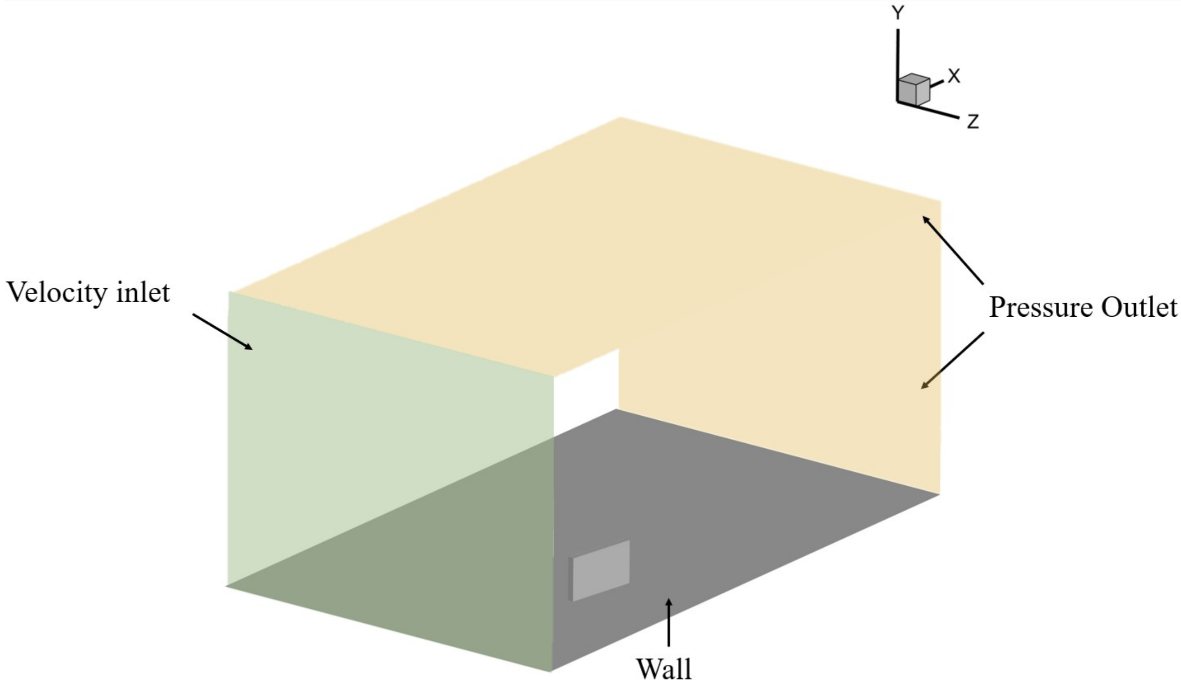

Figure 1. Overview of the computational domain, the green plane showing the inlet, orange showing outlets. The wall region with a single MVG is gray. Symmetry condition is applied on the side walls.

2.2. MVG Parameters and Flow Configuration

The C02 setup from Sattarzadeh and Fransson [21] serves as the base configuration for this study. The flow parameters are defined by a free-stream velocity of $U_\infty = 6\,\mathrm{m/s}$ and a kinematic viscosity of $\nu = 1.4607 \times 10^{-5}\,\mathrm{m^2/s}$, making comparison possible between the experimental results from the base case and the numerical simulations. The flow direction is along the x-axis, while y and z denote the wall-normal and spanwise directions, respectively.

The spanwise inner distance between the centers of two MVGs in a pair is denoted by d, and the spanwise distance between two pairs of MVGs is represented by Λ. Each MVG has a width (w), length (L), and height (h), and forms an angle (θ) with respect to the free-stream velocity. To extend the current parametric study, the height, inner distance, and spanwise periodicity are varied. The parameters include h ranging from [0.360:0.0554:0.526] $\delta_{99,MVG}$ and Λ covering [1.949:0.900:7.34] $\delta_{99,MVG}$, where the bracketed values denote the initial point, spacing, and endpoint of the parameter grid. The ratio d/λ varies between [0.2, 0.35, 0.5, 0.65, and 0.8]. This configuration results in a total of 140 cases. A schematic overview of all parameters is provided in Figure 2. Table 1 lists the values for these different parameters for the base case.

Table 1. Base parameters of the MVG setup.

h (mm)	Λ (mm)	**d** (mm)	**L** (mm)	**w** (mm)	Θ (°)	$X_{\mathbf{MVG}}$ (mm)	X_0 (mm)
1.3	13	3.25	3.25	0.3	9	222	213

Preprints.org (www.preprints.org) | NOT PEER-REVIEWED | Posted: 26 July 2024 doi:10.20944/preprints202407.2164.v1

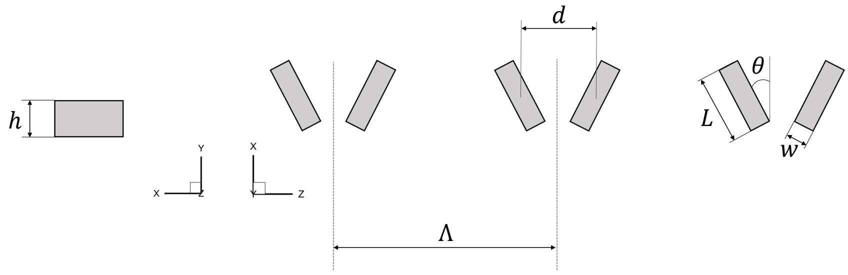

Figure 2. Schematic overview of MVG parameters.

2.3. Vortex Characterisation

As detailed in section 1, previous computational studies have primarily focused on boundary layer stabilization using free-stream vortices. The Batchelor vortex [11] serves as the model for an idealized free-stream vortex, with its velocity profile defined by

$$V_{\theta}(r,\theta) = \frac{\Gamma}{2\pi r}\left(1 - \exp\left(-\frac{r^2}{R_c^2}\right)\right). \tag{2}$$

In this formula, V_{θ} represents the tangential velocity component, corresponding to the V component in a horizontal profile or the W component in a vertical profile. Γ denotes the circulation, and R_c signifies the vortex radius. When analyzing realistic vortices, a method must be developed to compare these realistic vortices with their idealized counterparts. The generated vortex's velocity profiles are fitted along the average of a horizontal and vertical line through the vortex center to achieve this comparison using a non-linear least squares method. Although the position of maximum velocity remains consistent across both profiles, there is often a noticeable asymmetry in the vortex, depending on the specific case. This asymmetry arises from the influence of the bottom wall and the presence of the other vortex within the pair. The fitted Batchelor vortex used for comparison is based on the average of both profiles, accounting for these asymmetrical influences.

To quantify the asymmetry present in a vortex pair, a measure of asymmetry was developed for comparative analysis across different cases. By examining the velocity profiles of vortices in both horizontal and vertical directions, distinct peaks were observed, indicating the maximum or minimum speeds of the vortex in each direction. To assess asymmetry, the ratio of the horizontal to vertical distances between these peaks was calculated, defining the aspect ratio. Although this method primarily considers the horizontal and vertical planes, it provides a sufficient estimation of asymmetry, as the primary factor influencing asymmetry is the horizontal (bottom) wall. An aspect ratio of one implies that the peaks of the vortex velocity profiles in the horizontal and vertical direction are equidistant from the vortex center.

3. Results

In this section, the results of the vortex analysis are presented. Initially, the velocity profiles are displayed, followed by an overview of the vector map and the method used to determine the vortex center. Subsequently, heatmaps are presented to visualize the data across the different cases, as well as scatter plots comparing different parameters. These heatmaps and scatter plots offer a comprehensive depiction of the observed variations and patterns, enabling a comparative analysis. Lastly, Q criterion visualisations give a qualitative insight into the vortical structures.

3.1. Batchelor vortex fitting

To gain more information about the vortex center, the velocity fields are examined by plotting two lines: isocurves of the spanwise velocity subtracted by the upward velocity set to zero, and vice

Preprints.org (www.preprints.org) | NOT PEER-REVIEWED | Posted: 26 July 2024 doi:10.20944/preprints202407.2164.v1

versa. This method provides a robust approach to locating the vortex center, avoiding the influence of zero spanwise (w) or upward (v) velocity components near walls, as can be seen in Figure 3. Figure 4 presents an example of the velocity profiles along the horizontal and vertical lines through the vortex center, where the negative of the vertical velocity is plotted. This approach allows the two profiles to overlap, providing a clearer view of any asymmetry. Significant asymmetry would result in a large difference between the velocity profiles. A notable observation is the tendency of the W velocity profile to approach zero as it reaches the wall. These plots also illustrate the impact of low spanwise periodicity, which often causes the V velocity to not return to zero due to the influence of the adjacent vortex pair.

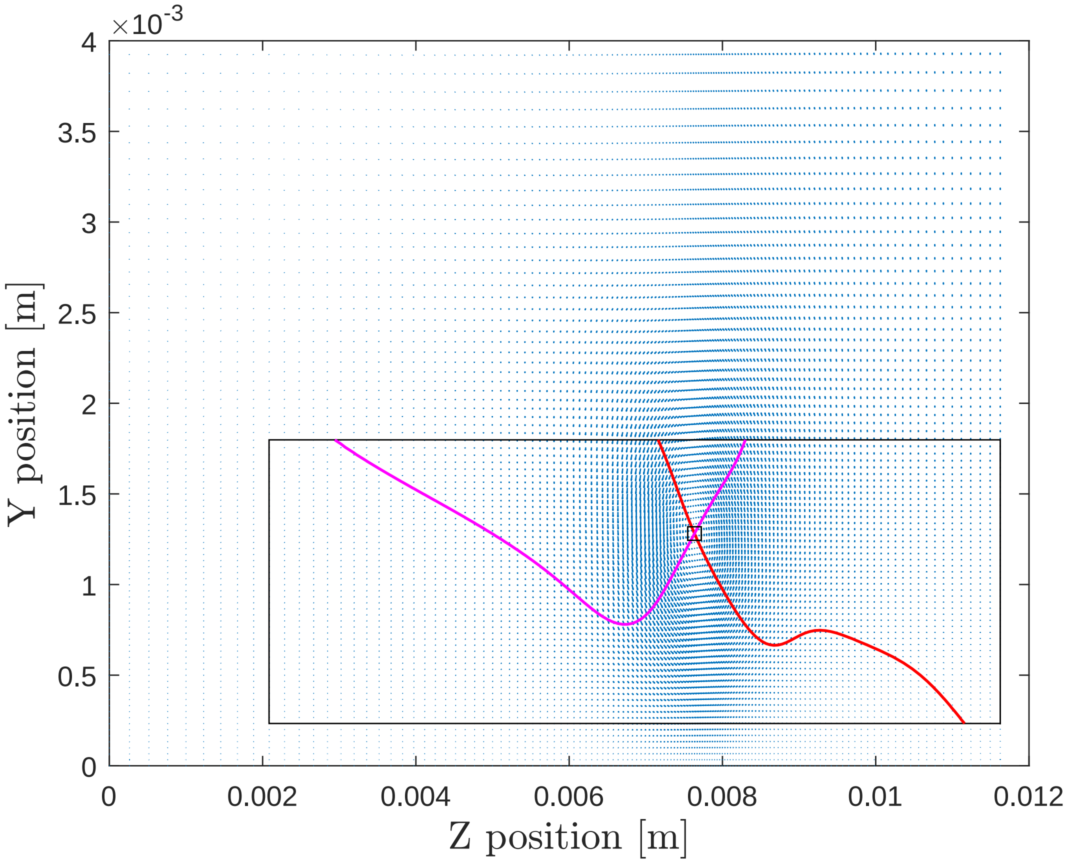

Figure 3. Vector plot showcasing the vortex contour intersection for finding vortex centers.

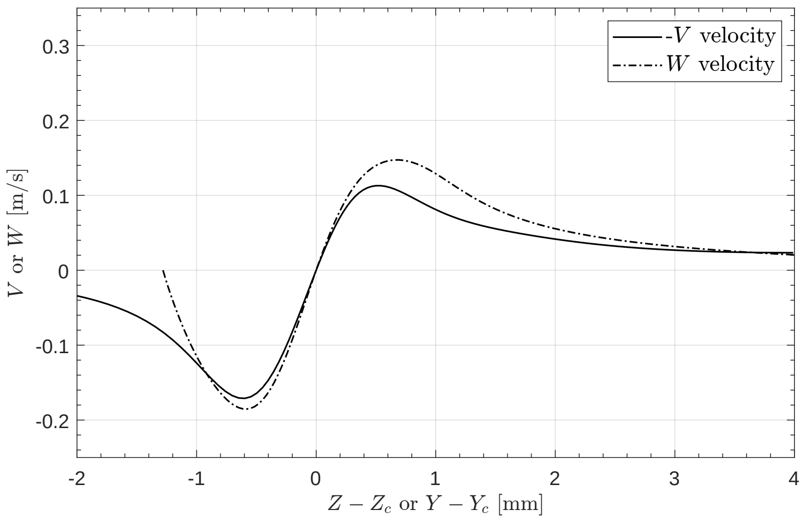

Figure 4. Horizontal and vertical velocity profiles through the vortex center.

As discussed in section 2.3, a Batchelor vortex is fitted to the average velocity profiles to compare the real vortices generated by the MVGs with an idealized vortex. Figure 5 illustrates this comparison, where the red line depicts the idealized vortex's velocity profile around the vortex core, and the blue line shows the average velocity of the actual vortex. This fitting process enables the estimation of important parameters, specifically circulation (Γ) and vortex radius (R_c).

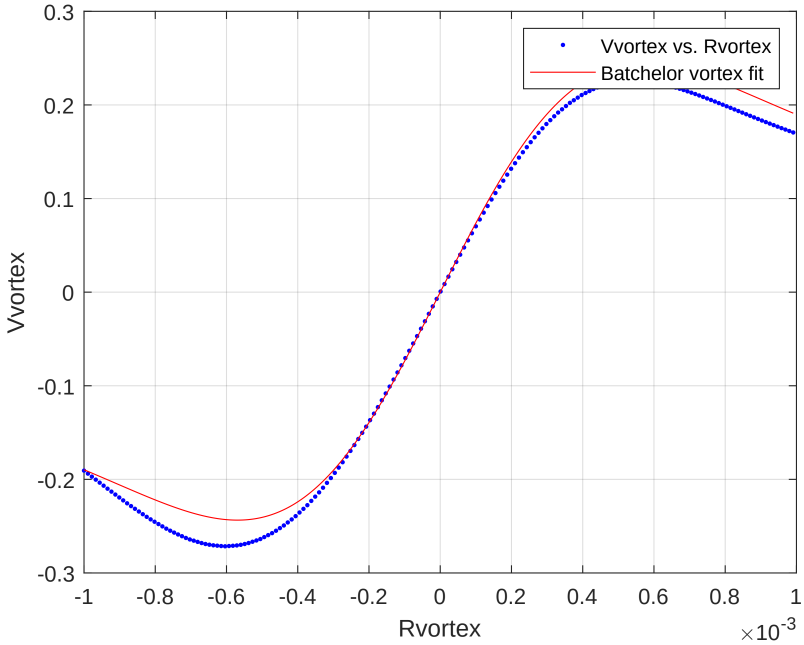

Figure 5. Comparing the averaged velocity profile (in blue) to the fitted Batchelor vortex profile (in red).

3.2. Heatmaps

The following section presents the analyzed vortex parameters. Heatmaps are made with spanwise periodicity (Λ) on the horizontal axis and the ratio of inner distance (d) to Λ on the vertical axis. Each heatmap corresponds to a specific MVG height indicated at the top of the figure. This arrangement allows for the visualization of various vortex characteristics, highlighting local peaks and overall trends. Comparing different figures provides insights into how the examined parameters vary across different MVG heights. The color scale for each parameter remains consistent across all cases.

doi:10.20944/preprints202407.2164.v1

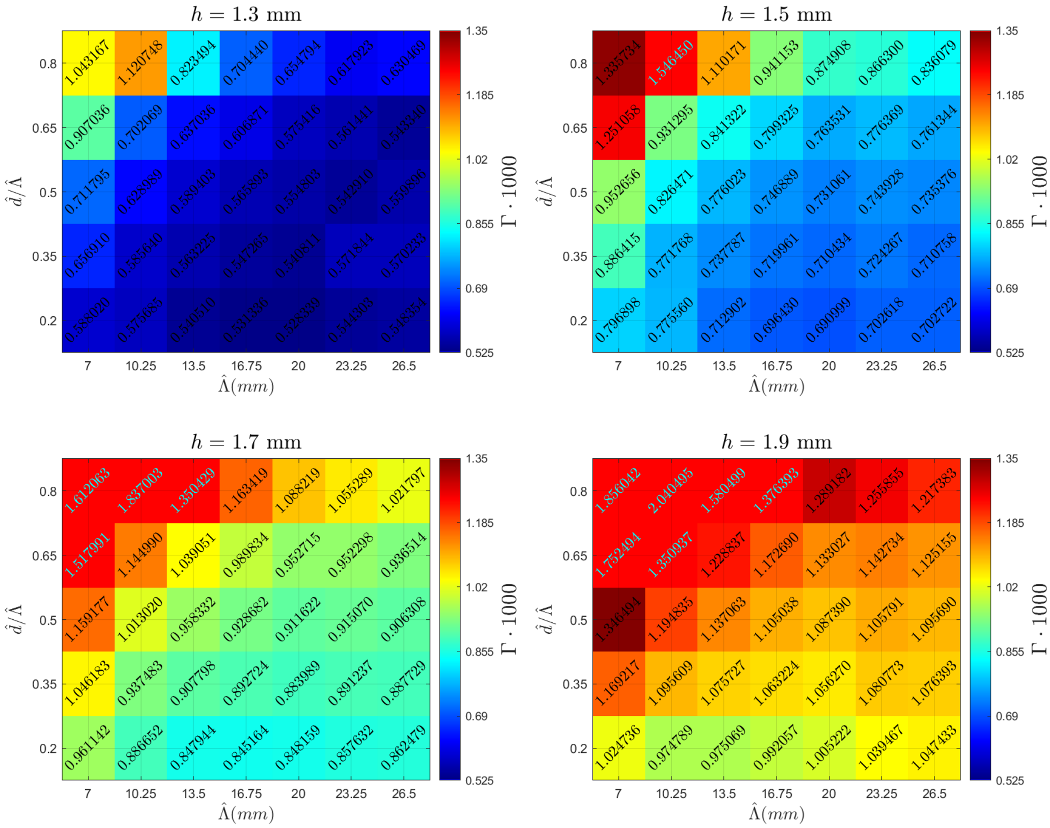

Figure 6. Case overview heatmap showcasing the value of circulation (Γ) for an MVG height of (**a**) 1.3 mm (**b**) 1.5 mm (**c**) 1.7 mm (**d**) 1.9 mm.

Preprints.org (www.preprints.org) | NOT PEER-REVIEWED | Posted: 26 July 2024 doi:10.20944/preprints202407.2164.v1

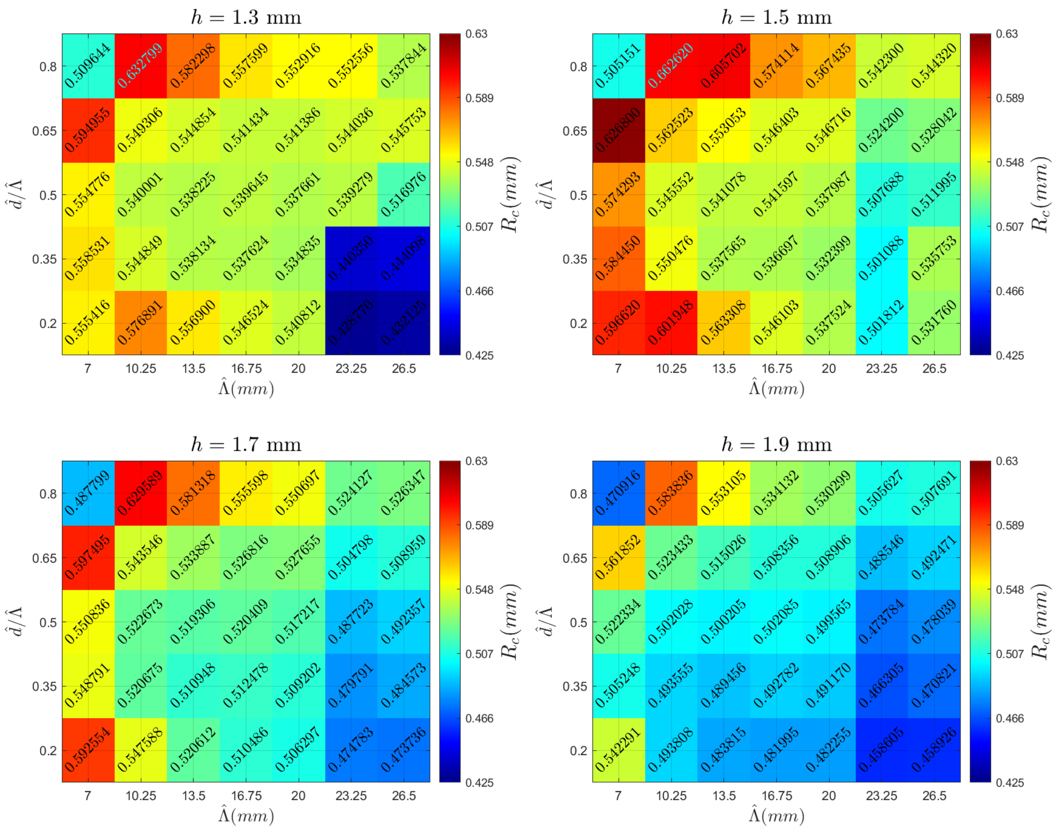

Figure 7. Case overview heatmap showcasing the value of vortex radius (R_c) for an MVG height of (**a**) 1.3 mm (**b**) 1.5 mm (**c**) 1.7 mm (**d**) 1.9 mm.

Preprints.org (www.preprints.org) | NOT PEER-REVIEWED | Posted: 26 July 2024 doi:10.20944/preprints202407.2164.v1

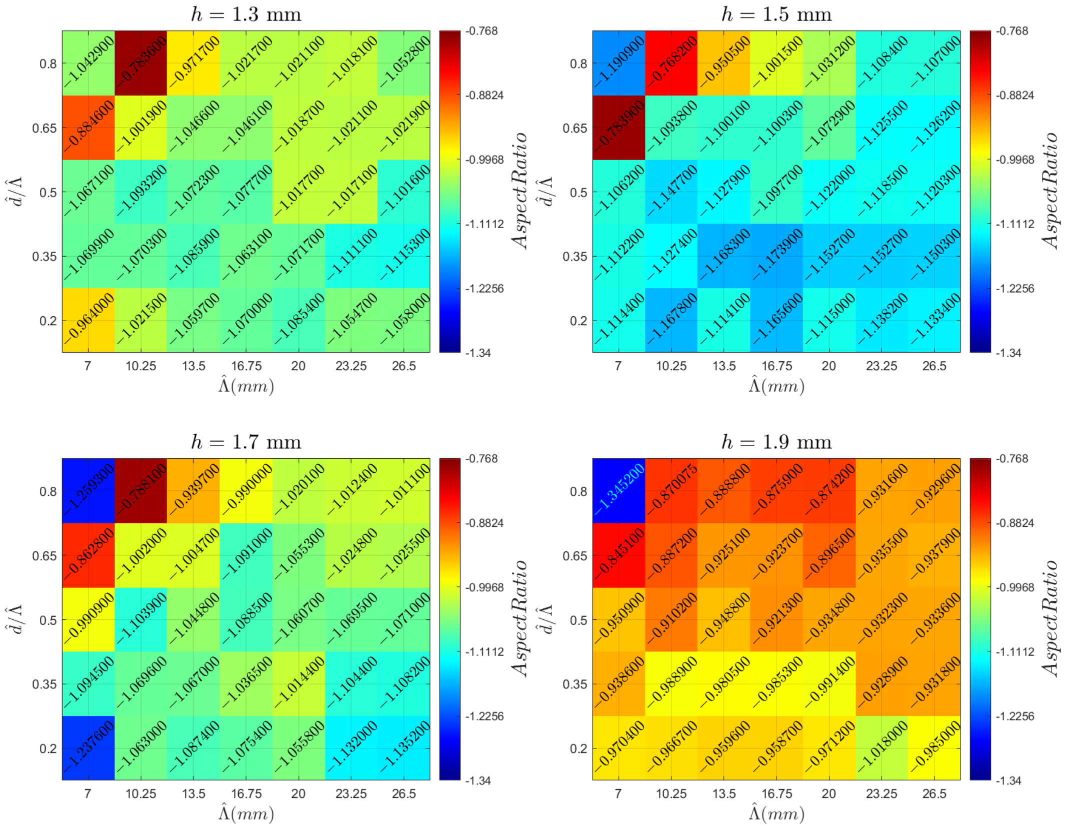

Figure 8. Case overview heatmap showcasing the value of vortex Aspect Ratio for an MVG height of (**a**) 1.3 mm (**b**) 1.5 mm (**c**) 1.7 mm (**d**) 1.9 mm.

Preprints.org (www.preprints.org) | NOT PEER-REVIEWED | Posted: 26 July 2024 doi:10.20944/preprints202407.2164.v1

3.3. Drag Reduction Potential and Correlation Maps

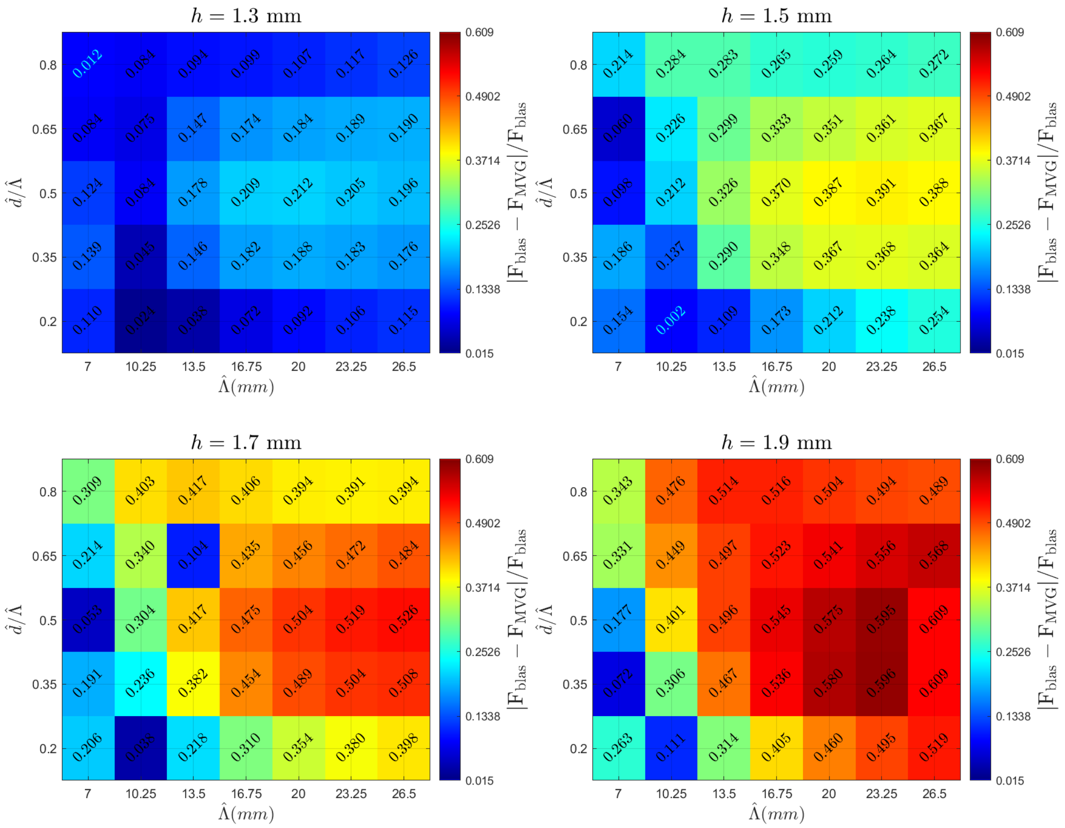

Figure 9. Case overview heatmap showcasing the decrease in force of a regular Blasius boundary layer compared to the flow field with MVGs present, based on the stability calculations in [19] for MVG heights of (**a**) 1.3 mm (**b**) 1.5 mm (**c**) 1.7 mm (**d**) 1.9 mm.

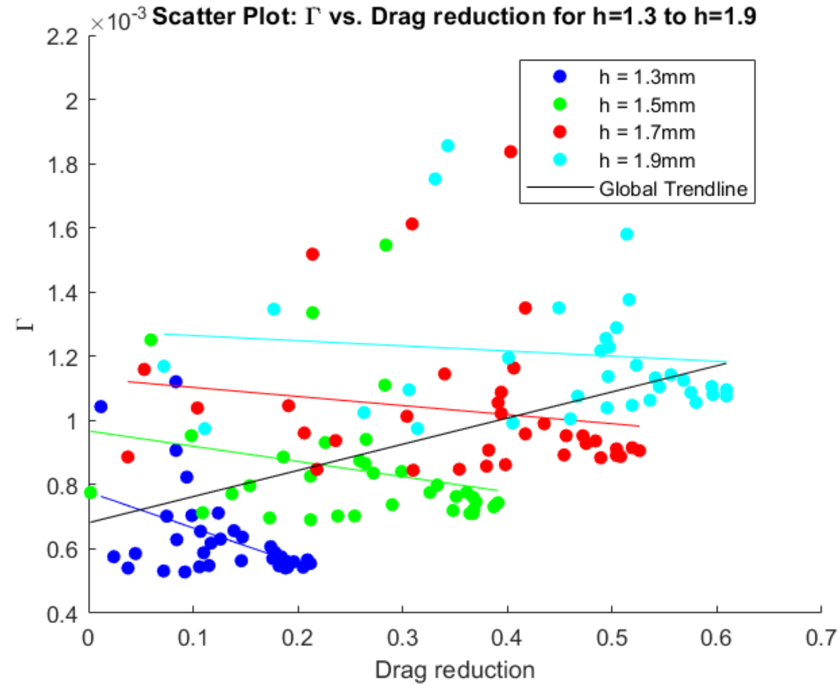

Figure 10. Scatter plot displaying drag reduction and circulation (Γ) for all cases.

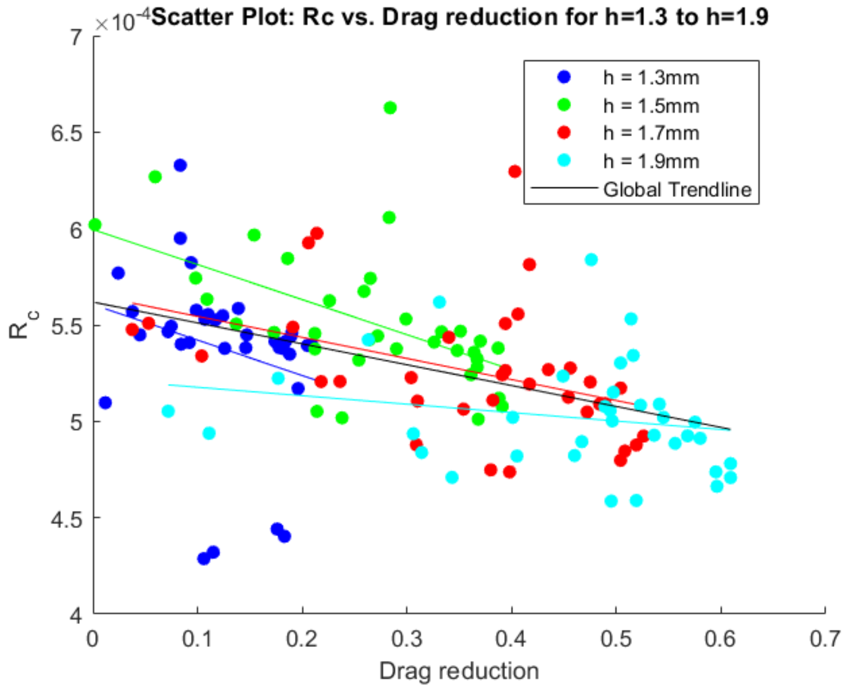

Figure 11. Scatter plot displaying drag reduction and radius of the vortex (R_c) for all cases.

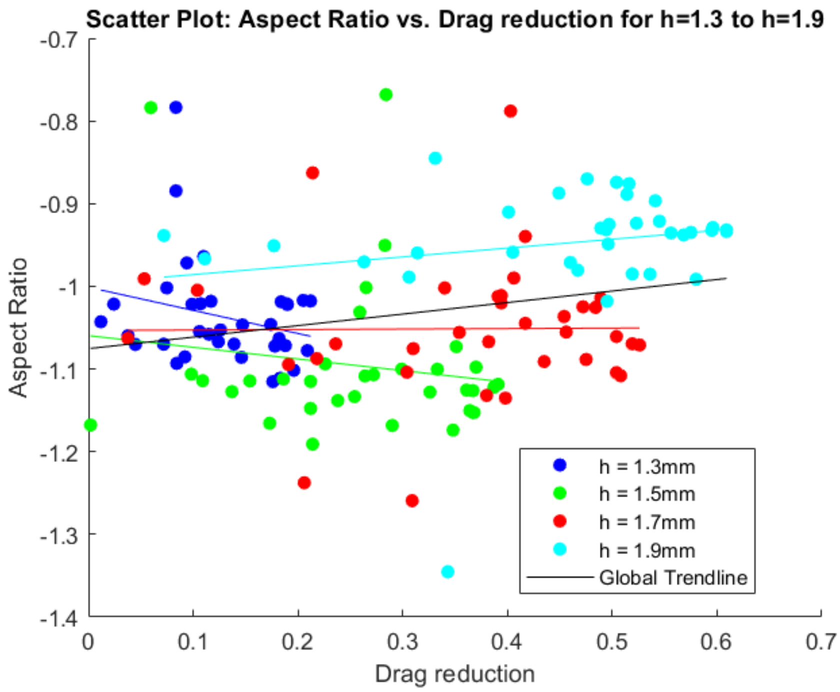

Figure 12. Scatter plot displaying drag reduction and Aspect Ratio for all cases.

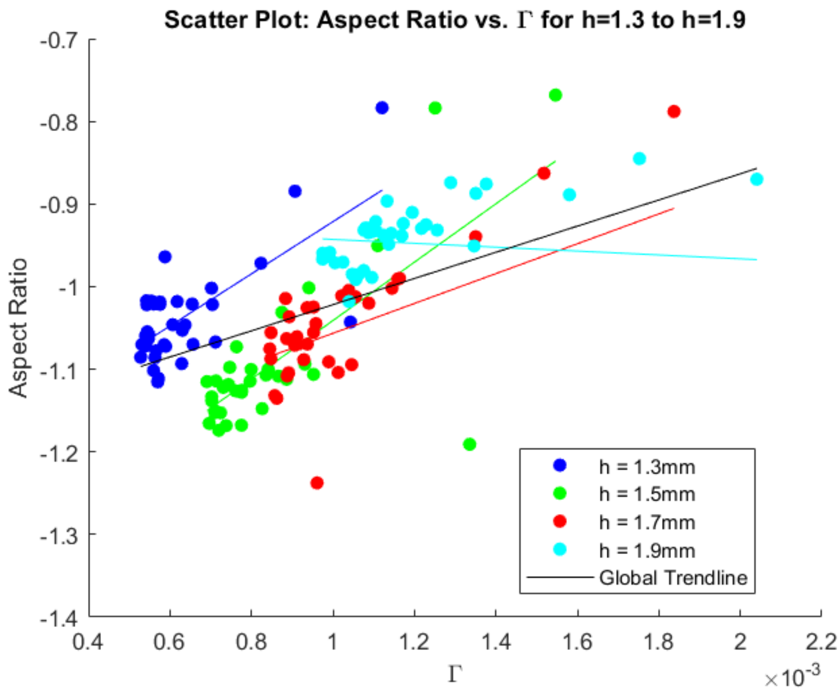

Figure 13. Scatter plot displaying circulation and aspect ratio for all cases.

3.4. Vortical Structure Analysis

To visually represent vortex strength in the near-field close to the MVG, a Q criterion analysis was conducted on all cases. Figure 14 presents a comparison between two different cases. The top case exhibits a much more pronounced vortical structure compared to the bottom case. Additionally, isosurfaces denoting zero streamwise velocity are observed. Although these isosurfaces do not provide direct numerical values regarding vortex size or strength, they offer a visual representation of these parameters, facilitating the linkage of calculated vortex parameters to the physical flow structure. In Figures 15 and 16, cross-sectional planes clearly show the interaction and effect of the analyzed vortices on the boundary layer. The "lift-up" mechanism, as described in section 1, is evident, and its strength varies depending on the MVG configuration. This visual analysis helps to better understand the relationship between MVG design and its impact on vortex behavior and boundary layer characteristics.

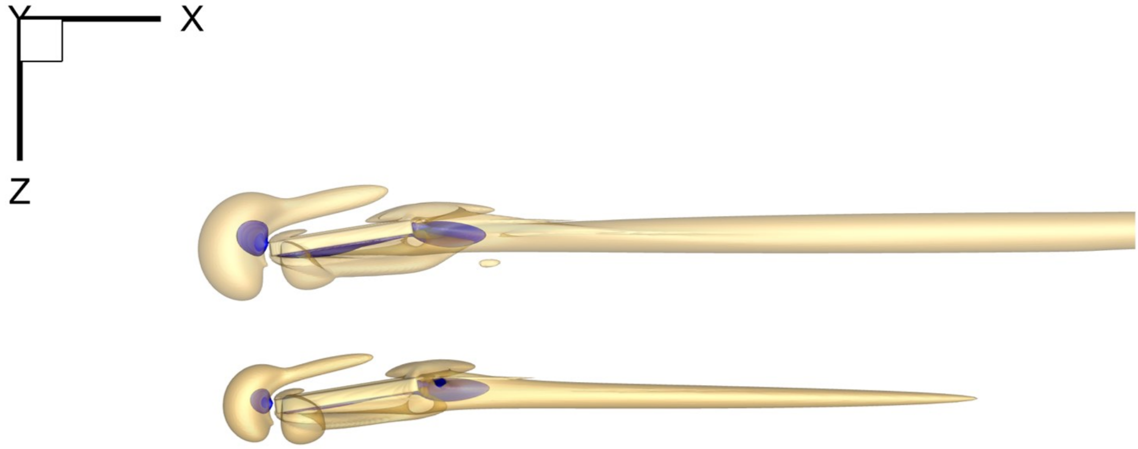

Figure 14. Comparison between two cases: Top view of the flow structure, with vortical structures visualised in yellow isosurfaces of Q = 1 x 10^5. In dark blue, regions of zero streamwise velocity are shown.

Preprints.org (www.preprints.org) | NOT PEER-REVIEWED | Posted: 26 July 2024 doi:10.20944/preprints202407.2164.v1

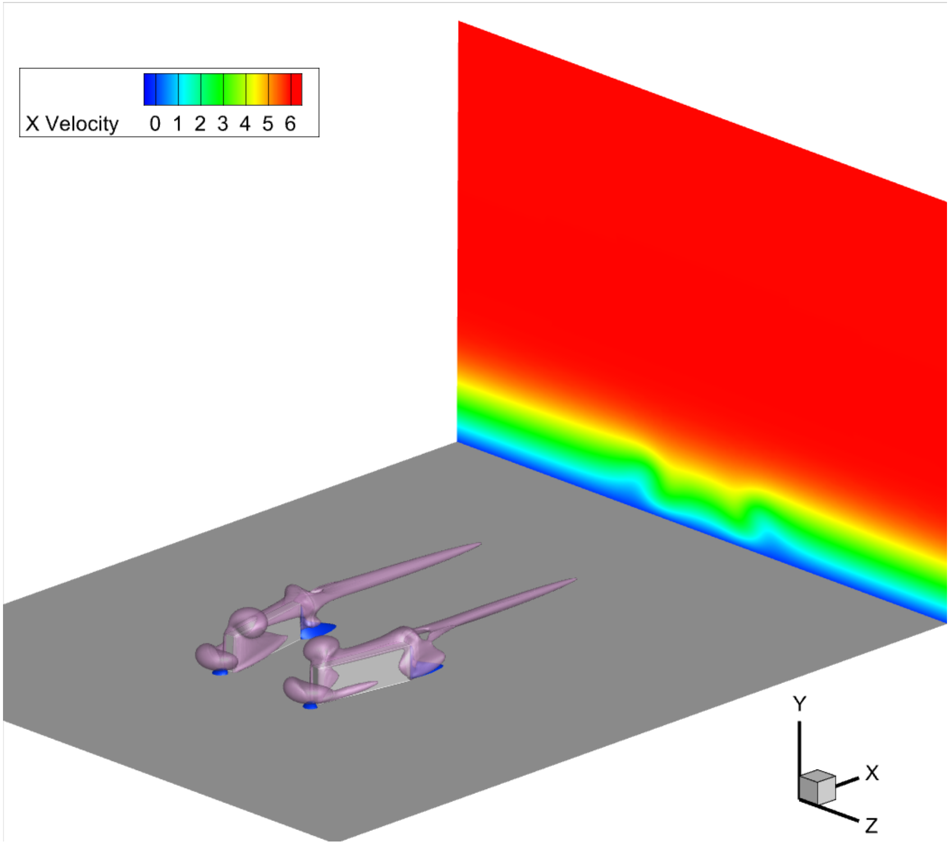

Figure 15. 3D visualisation of the near-field flow field, including purple isosurfaces of Q = 1 x 10^5. In dark blue, regions of zero streamwise velocity are shown and a cross-section of the velocity field at the end of the domain, showcasing the change in boundary layer.

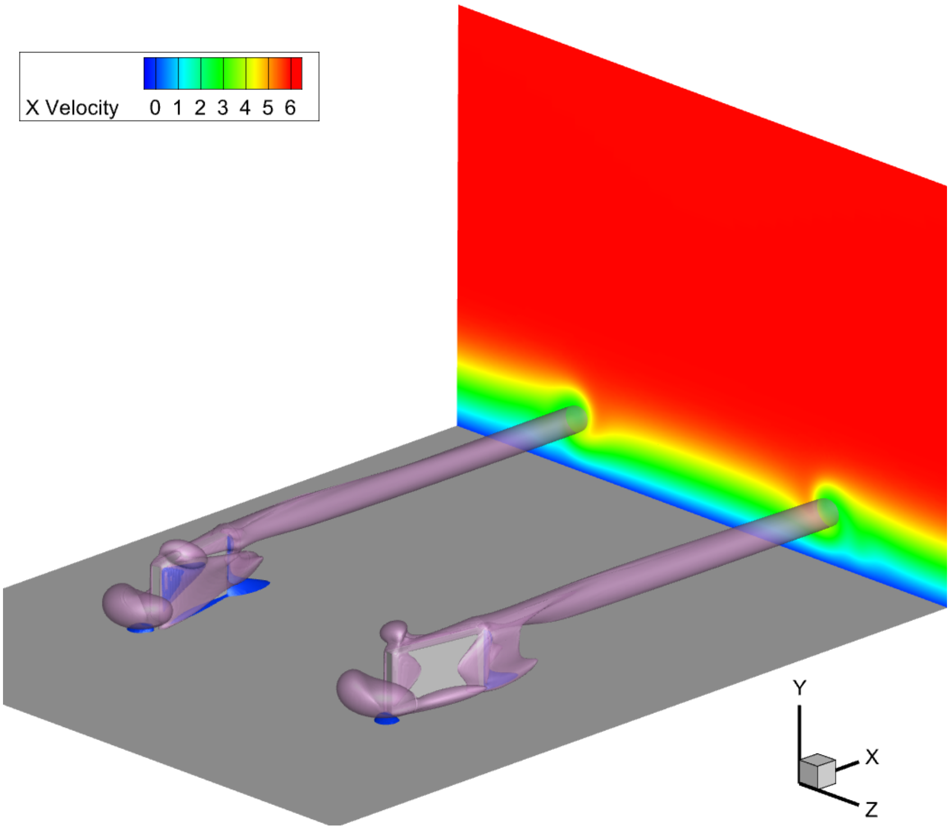

Figure 16. 3D visualisation of the near-field flow field, including purple isosurfaces of $Q = 1\,x\,10^5$. In dark blue, regions of zero streamwise velocity are shown and a cross-section of the velocity field at the end of the domain, showcasing the change in boundary layer.

4. Discussion

In this section, we discuss the initial conclusions that can be deducted from the dataset and plots presented above.

4.1. Circulation (Γ)

Examining the circulation values from Figure 10 reveals a distinct trend where circulation increases significantly with larger MVG height. This pattern is evident across all simulations, which were conducted with a consistent boundary layer height. As the height of the MVG increases, a larger portion of it is situated in the faster-moving region of the boundary layer. This interaction with the higher velocity flow increases the circulation value, leading to this trend. This relationship underscores the influence of MVG height on the vortex characteristics within the boundary layer.

When examining the trends for the same MVG height, as seen in the heatmaps of Figure 6, a peak is observed at lower lambda values and higher d over Λ values. This indicates that as the inner distance of the MVG pair increases, the circulation also increases, whereas the opposite is true for the periodicity values. Additionally, a link can be made to the results of Szabó *et al.* [19], where N factors are calculated. In short, the N factor essentially indicates the premature transition from laminar to turbulent flow. There is a strong correlation between circulation and the N factor. The reason for this is that a stronger vortex generates greater shear stresses in the boundary layer, which can accelerate flow destabilization. Furthermore, comparing circulation values to potential drag reduction downstream reveals a trend where higher drag reduction corresponds to higher circulation values. However, no clear trend is observed within the same MVG height, suggesting that circulation is not the primary factor in drag reduction. This presents an interesting dilemma, as circulation is crucial for assessing potential flow destabilization. Consequently, there is a limit to increasing the height of the MVGs

Preprints.org (www.preprints.org) | NOT PEER-REVIEWED | Posted: 26 July 2024 doi:10.20944/preprints202407.2164.v1

concerning its impact on circulation and flow stability. Understanding these relationships is essential for optimizing MVG design to balance drag reduction and flow stability.

4.2. Aspect Ratio

As described in 2.3, the shape of the vortex is analysed by means of an "aspect ratio", meaning the distance between the vortex' velocity profile peaks in the horizontal and vertical direction. Figure 17 shows an example of a strong asymmetrical vortex, how the vortex' velocity profile looks like in both directions and how this is visible on the vector plot, as seen in Figure 3. The plots of Figure 12 reveal a trend where the absolute value of the aspect ratio decreases from above 1 to below 1 as the MVG height increases, indicating a change in vortex shape with increasing MVG height. The aspect ratio is defined as the distance between the peaks in the Y direction over the distance between the peaks in the Z direction. This means that a low aspect ratio corresponds to a flatter elliptical shape of maximum velocity contours, while a higher aspect ratio indicates a more elongated (vertical) shape. Thus, increasing the MVG height results in a "flattening" of the vortex. The main reason for this can also be found in the velocity profiles themselves, as we see that the influence of the wall is far greater for lower MVG pairs.

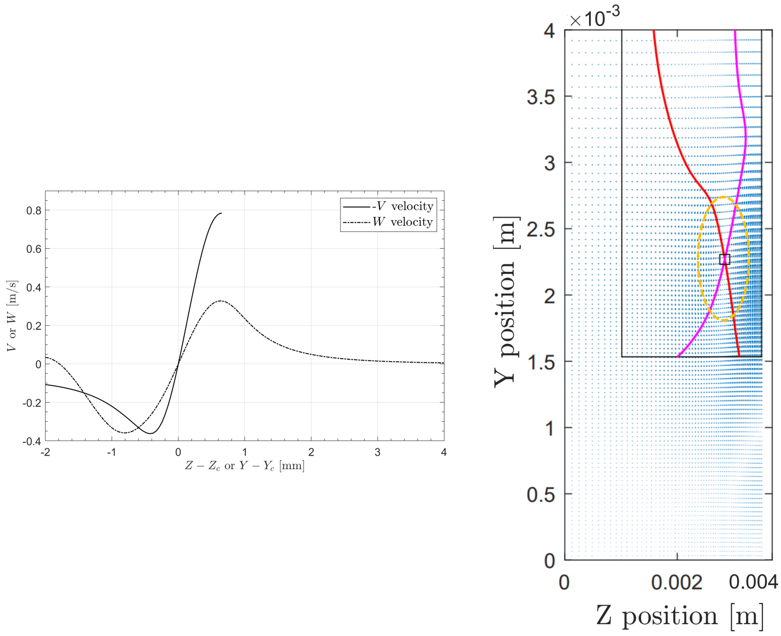

Figure 17. On the left, a vortex velocity profile plot, similar to Figure 4, with on the right a vector plot, similar to Figure 3. For this case, found in the heatmaps in Figure 8 at 1.9mm, top left, the absolute value of asymmetry is 1.345. In yellow the rough outline of the vortex shape is shown.

As can be seen in Figure 8, for a given MVG height, a greater spread between MVG pairs (higher periodicity) generally leads to lower aspect ratios, likely due to the reduced influence of adjacent MVG pairs. Placing single MVGs closer together tends to create flatter vortices, as the aspect ratio decreases with higher inner distance over periodicity values. There does not appear to be a strong correlation between aspect ratio and drag reduction, as seen in Figure 12, again indicating that this is not a crucial factor in optimal streak creation. However, a clear trend emerges when comparing aspect ratio to circulation values, shown on Figure 13. A lower aspect ratio, indicating a flatter vortex, corresponds to a higher circulation value. This observation aligns with the previously described analysis of circulation trends.

 doi:10.20944/preprints202407.2164.v1

4.3. Vortex Radius (R_c)

Interestingly, when examining the vortex radius for different MVG heights, data show that the radius generally decreases as the MVG height increases, as seen in Figure 11, indicating a more concentrated vortex core. Low periodicity values are a significant factor in increasing the vortex radius. Both effects are related to the previously described influence of the wall as well as adjacent vortex pairs on the vortex velocity profile. When vortex pairs are very close together, the velocity peaks shift, increasing the vortex diameter, showcased in Figure 7. Considering both asymmetry and radius values is crucial, as the Batchelor vortex fit assumes an axisymmetric vortex and does not account for strong asymmetrical effects. This limitation can result in outliers, particularly at the edges of the investigated domain. One of these outliers is analysed in Figure 17, where the high asymmetry also results in an R_c value that doesn't follow the general trend, meaning the asymmetry plays a big role for these outlier cases. A clear correlation exists between vortex radius and drag reduction: a lower radius tends to be more effective in achieving larger downstream drag reduction. The vortex radius significantly influences streak generation and amplitude, which are critical factors the attenuation of TS waves.

5. Conclusions

In conclusion, this vortex study of Miniature Vortex Generators (MVGs) on boundary layer flows showed significant insights into the possible changed MVG parameters and their effect on the downstream drag reduction, as well their effect on characteristics of the vortices themselves. This was then also linked to the possible downstream drag reduction. This analysis of vortex behavior shows the critical role of optimizing MVG configurations to achieve desired transition delay for drag reduction purposes. The key takeaway points can be summarised as:

MVG height compared to boundary layer height is one of the most important parameters, with notable changes in vortex characteristics observed for these different heights. Specifically, increased MVG height leads to a higher circulation and a reduction in vortex radius (Rc), whilst also "flattening" the vortex, meaning it has the tendency to be longer in the spanwise direction compared to the vertical direction. Elevated circulation values associated with higher MVGs also correlate with an increased risk of premature transition from laminar to turbulent flow, due to stronger vortices inducing higher shear stresses in the boundary layer, possibly destabilizing the flow. An optimal MVG height must thus be determined to balance performance and stability. While higher MVGs generally demonstrate improved performance in terms of delaying transition and reducing drag, they also exhibit higher circulation values. This increase in circulation makes the boundary layer more susceptible to bypass transition, which can negate the benefits of using MVGs. Therefore, a careful balance must be struck to maximize the aerodynamic advantages while minimizing the risk of unintended transition. Among the parameters studied, the vortex radius (Rc) emerged as the most crucial factor in achieving drag reduction. The correlation between Rc and drag reduction underscores the importance of managing vortex size to optimize aerodynamic efficiency.

In summary, the study underscores the complexity of optimizing MVG parameters to achieve desired aerodynamic outcomes. The interplay between MVG height, circulation, vortex shape, and transition risk necessitates a nuanced approach to design and implementation. Looking at the vortex characteristics themselves paves the way of defining a more optimized strategy in changing MVG parameters. Now, instead of changing physical parameters and having to conduct a stability analysis, one can look at the desired vortex characteristics and change the MVG parameters to suit this. Future research should further look into these (and possibly more) vortex characteristics and could also extend currently analyzed the parameter range. The insights gained from this investigation provide a valuable foundation for further advancements in boundary layer control and aerodynamic optimization.

Author Contributions: Conceptualization, G.D. and M.V.; methodology, G.D, A.S.,P.N., G.P. and M.V.; software, G.D., A.S., P.N. and M.V.; validation, G.D, A.S.,P.N., G.P. and M.V.; formal analysis, G.D.; investigation, G.D.; resources, A.S., P.N. and M.V.; data curation, G.D. and M.V; writing—original draft preparation, G.D.; writing—review and editing, G.D, A.S.,P.N. and M.V.; visualization, G.D.; supervision, M.V.; project administration,

G.P and M.V.; funding acquisition, G.P and M.V. All authors have read and agreed to the published version of the manuscript.

Funding: The authors gratefully acknowledge the funding of this research under the Celsa framework by grant No. CELSA/21/024.

Informed Consent Statement: Not applicable.

Data Availability Statement: Source data presented in this study are available on request from the corresponding author.

Conflicts of Interest: The authors declare no conflicts of interest.

References

1. Morkovin, M.V. On the Many Faces of Transition. Viscous Drag Reduction; Wells, C.S., Ed.; Springer US: Boston, MA, 1969; pp. 1–31.
2. Reshotko, E. Transient growth: A factor in bypass transition. *Physics of Fluids* **2001**, *13*, 1067–1075. doi:10.1063/1.1358308.
3. Tollmien, W. Über die Entstehung der Turbulenz. 1. Mitteilung. *Nachrichten von der Gesellschaft der Wissenschaften zu Göttingen, Mathematisch-Physikalische Klasse* **1928**, *1929*, 21–44.
4. Kachanov, Y.S. Physical Mechanisms of Laminar-Boundary-Layer Transition **1994**.
5. Gad-el Hak, M. Flow Control. *Applied Mechanics Reviews* **1989**, *42*, 261–293. doi:10.1115/1.3152376.
6. Fransson, J.H.M.; Brandt, L.; Talamelli, A.; Cossu, C. Experimental and theoretical investigation of the nonmodal growth of steady streaks in a flat plate boundary layer. *Physics of Fluids* **2004**, *16*, 3627–3638. doi:10.1063/1.1773493.
7. Landahl, M.T. On sublayer streaks. *Journal of Fluid Mechanics* **1990**, *212*, 593–614. doi:10.1017/S0022112090002105.
8. Brandt, L.; Henningson, D.S. Transition of streamwise streaks in zero-pressure-gradient boundary layers. *Journal of Fluid Mechanics* **2002**, *472*, 229–261. doi:10.1017/S0022112002002331.
9. Siconolfi, L.; Camarri, S.; Fransson, J.H.M. Stability analysis of boundary layers controlled by miniature vortex generators. *Journal of Fluid Mechanics* **2015**, *784*, 596–618. doi:10.1017/jfm.2015.591.
10. Fransson, J.H.M.; Talamelli, A.; Brandt, L.; Cossu, C. Delaying Transition to Turbulence by a Passive Mechanism. *Physical Review Letters* **2006**, *96*, 064501. doi:10.1103/PhysRevLett.96.064501.
11. Batchelor, G.K. Axial flow in trailing line vortices. *J. Fluid Mech. 20* **1964**, pp. 645–658.
12. De Tullio, N.; Paredes, P.; Sandham, N.D.; Theofilis, V. Laminar–turbulent transition induced by a discrete roughness element in a supersonic boundary layer. *Journal of Fluid Mechanics* **2013**, *735*, 613–646. Edition: 2013/10/29 Publisher: Cambridge University Press, doi:10.1017/jfm.2013.520.
13. Konishi, Y.; Asai, M. Experimental investigation of the instability of spanwise-periodic low-speed streaks. *Fluid Dynamics Research* **2004**, *34*, 299–315. doi:https://doi.org/10.1016/j.fluiddyn.2004.02.003.
14. Fransson, J.H.M.; Brandt, L.; Talamelli, A.; Cossu, C. Experimental study of the stabilization of Tollmien–Schlichting waves by finite amplitude streaks. *Physics of Fluids* **2005**, *17*, 054110. doi:10.1063/1.1897377.
15. Shahinfar, S.; Fransson, J.H.M.; Sattarzadeh, S.S.; Talamelli, A. Scaling of streamwise boundary layer streaks and their ability to reduce skin-friction drag. *Journal of Fluid Mechanics* **2013**, *733*, 1–32. doi:10.1017/jfm.2013.431.
16. Shahinfar, S.; Sattarzadeh, S.S.; Fransson, J.H.M.; Talamelli, A. Revival of Classical Vortex Generators Now for Transition Delay. *Physical Review Letters* **2012**, *109*, 074501. doi:10.1103/PhysRevLett.109.074501.
17. Siconolfi, L.; Camarri, S.; Fransson, J.H.M. Boundary layer stabilization using free-stream vortices. *Journal of Fluid Mechanics* **2015**, *764*, R2. doi:10.1017/jfm.2014.731.
18. De Baets, G.; Szabo, A.; Nagy, P.T.; Paal, G.; Vanierschot, M. Vortex Characteristics of Miniature Vortex Generators: A Numerical Investigation. In proceedings of the Canadian Society for Mechanical Engineering International Congress 31st Annual Conference of the Computational Fluid Dynamics Society of Canada; , 2024.
19. Szabó, A.; Nagy, P.T.; De Baets, G.; Vanierschot, M.; Paál, G. Stability analysis of a streaky boundary layer generated by miniature vortex generators. *Computers & Fluids* **2024**, *269*, 106123. doi:10.1016/j.compfluid.2023.106123.

20. Camarri, S.; Fransson, J.H.M.; Talamelli, A. Numerical Investigation of the AFRODITE Transition Control Strategy. In *Progress in Turbulence V*; Talamelli, A.; Oberlack, M.; Peinke, J., Eds.; Springer International Publishing: Cham, 2014; Vol. 149, pp. 65–69. Series Title: Springer Proceedings in Physics, doi:10.1007/978-3-319-01860-7_11.
21. Sattarzadeh, S.S.; Fransson, J.H.M. On the scaling of streamwise streaks and their efficiency to attenuate Tollmien–Schlichting waves. *Experiments in Fluids* **2015**, *56*, 58. doi:10.1007/s00348-015-1930-x.